Int. J. Heat Mass Transfer. Vol. 31, No. 11, pp. 2197–2205, 1988
Printed in Great Britain

0017-9310/88 $3.00+0.00

Experiments on natural convection in divergent vertical channels and correlation of divergent, convergent, and parallel-channel Nusselt numbers

E. M. SPARROW and R. RUIZ
Department of Mechanical Engineering, University of Minnesota, Minneapolis, MN 55455, U.S.A.

(*Received* 29 *January* 1988 *and in final form* 10 *May* 1988)

Abstract—The objectives of this investigation are to obtain definitive heat transfer data for natural convection in divergent vertical channels, to visualize the flow in the channels, and to develop a universal Nusselt number correlation for divergent, convergent, and parallel-walled channels. The experiments are performed with water as the working fluid ($Pr \sim 5$) and are parameterized by the angle of divergence of the channel, the ratio of the channel length to minimum cross section, and the product of the Rayleigh number and the cross section/length ratio. Temperature uniformity is maintained at the channel walls, and the wall temperature exceeds the temperature of the fluid environment. The flow visualization reveals the presence of a recirculation zone which extends downward from the exit into the channel, but the Nusselt numbers are found to be independent of the extent of the downward penetration of the recirculation zone. The measured Nusselt numbers for the divergent channel are brought into tight correlation with those for the convergent and parallel-walled channels by using correlating parameters based on the maximum interwall spacing as the characteristic dimension. The correlation is conveyed by equation (4) ($Nu_{S_{max}} = 0.740[(S_{max}/L)Ra_{S_{max}}]^{0.240}$).

INTRODUCTION

THIS PAPER is concerned with the buoyancy-induced fluid flow and heat transfer in a plane-walled vertical channel the cross-sectional area of which increases in the upward direction. Both the lower and upper ends of the channel are open to a large, all-encompassing fluid environment which is at a uniform temperature T_∞. The principal walls of the channel are at a common uniform temperature T_w which exceeds T_∞. A schematic diagram of the physical situation is presented in Fig. 1.

The channel shown in Fig. 1 will be termed a divergent channel. Since such a designation is usually employed to describe a channel in which the cross-sectional area increases in the direction of fluid flow, its use here may suggest that there is a vertical upflow in the channel. As will be demonstrated later, there is, indeed, a *net* vertical upflow, thereby justifying the channel being designated as divergent. There is, however, a substantial zone of downflow within the channel.

The lower end of the channel is strictly an inflow cross section (i.e. upflow only), and the experimental apparatus was designed to have a sharp-edged inlet, as shown in Fig. 1. On the other hand, the upper end of the channel is both an inflow and outflow cross section, with inflow (downflow) in the central portion of the cross section and outflow (upflow) in the remaining portion.

The elaboration of the aforementioned fluid flow features constitutes one aspect of the experimental work to be reported here. For this part of the research, flow visualization experiments are performed using the thymol blue technique. This technique is based on creating, by electrochemical means, a local change in the pH of the fluid. In the presence of thymol blue, a pH indicator, the local change in pH results in a local color change of the fluid. The color-changed fluid is neutrally buoyant and faithfully follows the flow pattern.

The other part of the research is focused on the determination of average heat transfer coefficients and Nusselt numbers and on the unification of these results with those for convergent and parallel-walled

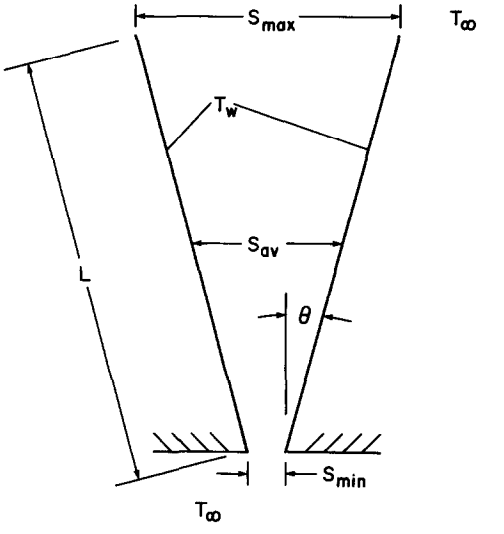

FIG. 1. Schematic diagram of the divergent flow channel.

NOMENCLATURE

A	surface area of the heated walls	T	temperature
g	acceleration of gravity	T_w	wall temperature
h	average heat transfer coefficient, $Q/A(T_w-T_\infty)$	T_∞	temperature of fluid environment
k	thermal conductivity	W	width of divergent walls
L	streamwise length of divergent wall	Z_A	vertical distance between bottom of recirculation zone and lower opening of channel.
Nu_ξ	Nusselt number, $h\xi/k$		
Pr	Prandtl number		
Q	heat transfer rate at the divergent walls		
Ra_ξ	Rayleigh number, $[g\beta(T_w-T_\infty)\xi^3/\nu^2]Pr$	Greek symbols	
S	spacing between channel walls	β	coefficient of thermal expansion
S_{av}	mean interwall spacing	θ	half angle of divergence
S_{max}	maximum interwall spacing	ν	kinematic viscosity
S_{min}	minimum interwall spacing	ξ	characteristic dimension.

vertical channels. The heat transfer experiments were performed as a function of three parameters. Two of these are geometrical—the half angle of divergence θ and the L/S_{min} ratio. These quantities are illustrated in Fig. 1, where L is seen to be the streamwise length of either principal wall, and S_{min} is the interwall spacing at the lower end of the channel (i.e. the minimum interwall spacing). For the experiments, θ took on values of 5, 10, and 15°, while the investigated values of L/S_{min} were 11.4 and 22.9. Figure 1 corresponds to $\theta = 15°$ and $L/S_{min} = 11.4$. It is readily seen that a 15° half angle corresponds to a high degree of divergence.

The other parameter that was varied during the heat transfer experiments is $(S/L)Ra_S$, where Ra_S is the Rayleigh number based on the interwall spacing S. The form of this parameter first arose from the analysis of the parallel-walled vertical channel. It has also served effectively as a correlation variable for convergent vertical channels [1]. There is, therefore, ample motivation for its use here. In the search for unifications between the present divergent-channel results and those for the convergent and parallel-walled channels, the $(S/L)Ra_S$ parameter will be separately evaluated for $S = S_{min}$, $S = S_{av}$, and $S = S_{max}$, all of which are illustrated in Fig. 1. The ranges of the three forms of $(S/L)Ra_S$ will be evident from the graphical presentation of results.

The Prandtl number was virtually a constant throughout the experiments. The participating fluid was water, and the temperature levels were set so that the Prandtl number was approximately equal to 5.

Another issue addressed in the paper was the observation that the flow pattern in the core of the channel evolved progressively over a long period of time (i.e. several hours) while the heat transfer coefficients were completely steady.

As noted earlier, the ultimate goal of the research is to bring together the Nusselt number results for the divergent, convergent, and parallel-walled vertical channels, so that a single representation applies for all. Based on available information for the convergent channel [1], the *a priori* probability for fulfilling this objective is not favorable. This is because the flows in the convergent and divergent channels are markedly different. For the former, the flow is unidirectional (i.e. upward) at all points in all cross sections. However, for the latter, there is both upflow and downflow at many cross sections in the channel.

It was the desire to seek a universal correlation that motivated the present research. It is appropriate to regard this research as a follow-on and a conclusion to what was reported by the authors in ref. [1] for the convergent vertical channel.

The only prior work on divergent vertical channels known to the authors is the numerical study of ref. [2]. The model used in ref. [2] was overly restrictive, so that only unidirectional flow was predicted for the range of half angles investigated here.

EXPERIMENTAL APPARATUS AND PROCEDURE

Figure 1 illustrates the physical situation under investigation but does not convey the details of the experimental apparatus. The general configuration of the apparatus can be seen in Fig. 2, which also serves to portray the results of the flow visualization that will be elaborated later. For now, Fig. 2 will be used to assist in the description of the apparatus. Since the present experiments are the divergent-channel counterpart of the convergent-channel investigation of ref. [1], the present apparatus is an adaptation of that of ref. [1]. Therefore, it will be sufficient to describe only the main features of the apparatus here.

The sloping walls shown in Figs. 1 and 2 constitute the principal walls of the flow passage. These walls were thermally active and were maintained at the same uniform temperature T_w. Uniformity was achieved by making the walls from 0.635-cm-thick copper plate

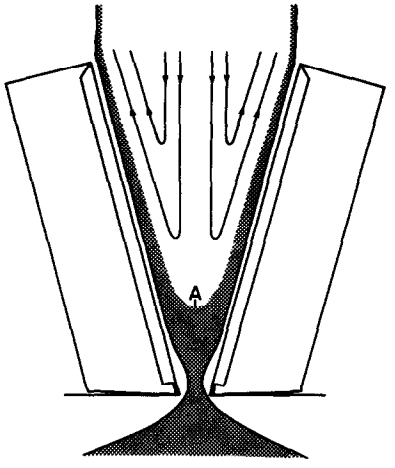

FIG. 2. Flow visualization pattern.

and by using three independently controlled heating circuits for each wall. Heating was accomplished electrically by a resistance wire embedded in grooves in the rear face of each plate. The streamwise length L of the plates was 14.52 cm, and their width W normal to the plane of the figures was 9.67 cm.

Each copper plate was backed by a 3.5-cm-thick block of water-tolerant Styrofoam insulation (Fig. 2). Note that the lower and upper ends of the plates were contoured to enable the insulation to cover the ends. The insulation was highly effective in suppressing extraneous heat losses. The Styrofoam block was, in turn, backed by a plexiglass plate for structural purposes (not shown).

As indicated in Fig. 1 and elaborated in Fig. 2, the opening at the lower end of the channel (i.e. the channel inlet) was a slit-like aperture in a horizontal wall. The horizontal framing of the opening was adopted as a standard condition for all the investigated angles of divergence. This condition was implemented by beveling back the lower end of each Styrofoam block as illustrated in Fig. 2 and then forming the horizontal wall from high-strength adhesive tape anchored to the tip of the copper plate and to the side walls of the flow channel.

The two side walls of the channel were vertical and made of 1.27-cm-thick plexiglass. These walls were thermally passive (i.e. unheated).

The channel geometry was set by fixing the spacing S_{min} (either at 0.635 or 1.27 cm) and the half angle of divergence θ (5, 10, and 15°). The other indicated interwall spacings S_{av} and S_{max} were not set independently but followed from S_{min}, θ, and L.

The flow channel was centrally positioned in a large plexiglass-walled tank filled with distilled water. The tank dimensions were $74 \times 43 \times 44$ cm (length $\times$ width $\times$ height). As a result of the central positioning, the lower opening of the channel was about 12.7 cm above the floor of the tank, while the upper opening was situated a similar distance below the free surface of the water. There were no obstructions of any kind in the neighborhood of either opening of the channel, so that fluid could pass freely from/to the tank to/from the channel.

The water-filled tank which housed the flow channel was thermally guarded by a tank-in-tank arrangement. This was accomplished by positioning the tank within a still larger plexiglass tank so that the intertank space was filled with temperature-controlled distilled water, with the temperature level set and maintained by an immersed controller–circulator unit. The open tops of both tanks were closed by a sheet of Styrofoam insulation lined with a vapor barrier.

Temperature measurements were made in each of the heated plates, in the fluid environment which surrounded the flow channel, and in the inter-tank space. Each plate was equipped with eight fine-gage, specially calibrated thermocouples with junctions situated only 0.05 cm from the exposed face of the plate. The temperature of the fluid environment was measured by a vertical array of three thermocouples located about 13 cm to the side of the flow channel, well away from the heated stream which exited the channel. The respective thermocouples of the array were 7.6, 16.5, and 24.1 cm above the floor of the tank.

A pair of 0.1°F thermometers, one in the main tank and the other in the intertank space, were placed adjacent to each other on either side of the plexiglass wall of the main tank. These thermometers were used during the procedure for establishing temperature equality of the water in the main and inter-tank spaces.

The procedure for establishing the temperature uniformity and quiescence in the fluid environment is detailed elsewhere [3]. The conditions which were met prior to the initiation of a data run included temperature equality of the paired thermometers, of the vertical array of thermocouples in the fluid environment, and of the thermocouples in the copper walls of the channel. These conditions guaranteed the absence of extraneous buoyant motions. Furthermore, about an hour was allowed for extraneous motions associated with the stirring of the fluid to die away.

A data run was initiated by providing electric power to the heating wires embedded in the channel walls. Steady-state thermal operation, as reflected by steady values of the wall and fluid environment temperatures, was achieved in less than 15 min, and the reported heat transfer coefficients are based on data collected during that period. Furthermore, during the data collection period, both wall temperature and fluid temperature uniformity were excellent. Deviations of individual wall temperature measurements from the wall average did not exceed 1% of the wall-to-ambient temperature difference. Similarly, deviations of individual fluid temperatures from the fluid average were confined to 1%. Longer runs, performed in connection with the flow visualization, displayed greater fluid temperature stratification, as will be discussed shortly.

FLOW VISUALIZATION

As was noted in the Introduction, the flow visualization was performed by making use of the thymol blue technique. This is an electrochemical technique in which a change in the color of the fluid is produced by changes in pH brought about by an imposed d.c. voltage. The thus-generated, colored tracer fluid is neutrally buoyant and precisely follows the pattern of fluid flow.

To enable the desired change of color to take place, minute amounts of three substances were added to the water. These are: an acid (hydrochloric acid), a base (sodium hydroxide), and a pH indicator (thymol blue). The thymol blue powder was first dissolved in a beaker containing distilled water and then added to the water in the main tank. The solution in the tank was homogenized by vigorous stirring and then titrated to the end point with the addition of sodium hydroxide. At this stage, the color of the solution is a deep blue. Next, hydrochloric acid was added to make the solution slightly acidic, as indicated by a color change from blue to yellow–orange.

If a small d.c. voltage (4–6 V) from an adjustable supply is applied across two electrodes situated in the solution, an electrochemical reaction will take place, and the pH of the solution in the neighborhood of the negative electrode will change from acidic to basic. This change of pH is accompanied by a change in color (yellow–orange to blue), as noted in the foregoing. It was found by experience that the imposition of less than 4 V did not generate sufficient amounts of colored tracer fluid to make the flow pattern visible. An imposed voltage in excess of 6 V not only produced unwanted hydrogen bubbles at the negative electrode, but also heated the electrode and thereby caused extraneous buoyancy.

In the present experiments, various negative electrodes were used in order to view different portions of the flow field. These included the copper walls of the flow passage and wire probes positioned at the lower and upper openings of the channel and in the core of the channel. The positive electrode was a large copper plate situated on the floor of the tank. The preparatory steps for a visualization run were identical to those for a heat transfer data run.

A diagram of the salient features of the flow field is presented in Fig. 2. The diagram conveys a composite view based on extensive visual observations. As will be elaborated shortly, it depicts a quasi-steady picture. In the diagram, the shaded areas are regions of virtually stagnant or very low velocity fluid where a definite direction of motion could not be discerned. In the unshaded areas, it was possible to positively identify the direction of fluid flow. The shaded areas are seen to form a wishbone-shaped configuration.

The lower opening of the channel is characterized by a non-uniform flow field. Fluid entering the channel is confined to narrow regions adjacent to the respective principal walls, with virtually stagnant fluid filling the central part of the inlet cross section. Since the entering fluid does not come from directly below the inlet, but rather comes from the sides, it possesses a significant transverse velocity component directed toward the axis of the channel as it passes through the opening. As a consequence, the entering flow intrudes into and pinches the stagnant core just above the opening. Subsequently, the just-entered fluid is drawn toward the walls because of the large near-wall buoyancy forces and, when this happens, the pinching of the core is relieved.

Thereafter, the bottom-entered fluid continues to move upward along the respective principal walls, forming a boundary layer adjacent to each wall. The flow in the boundary layer appears to be essentially parallel to the wall, and there was no observed tendency for the boundary layer to separate from the wall. Indeed, there was no significant streamwise growth of the boundary layer thickness. At the top of the channel, the fluid in the respective boundary layers departs the wall, becomes a plume, and continues to move upward, albeit with some waviness.

Further inspection of Fig. 2 reveals that fluid not only enters the lower opening of the channel, but that there is also an inflow of fluid into the channel through the upper opening. The inflow (i.e. downflow) at the top of the channel occupies the central part of the cross section, while outflow (i.e. upflow) occurs in the remainder of the cross section.

As indicated schematically in the figure, the downflow penetrates part way into the channel and then reverses direction, after which it becomes an upflow and exits the channel. This downflow–upflow recirculation zone is quite distinct from the wall-adjacent boundary layers. It is quite possible that there is some transverse fluid flow at the interfaces between the loop and the boundary layers, but such a flow could not be detected. The aforementioned flow reversal is believed due to the opposition of the bottom-entered upflow to further penetration by the top-entered downflow. The virtually stagnant region between these flows represents a neutral zone.

The numerically predicted flow fields of ref. [2] for the range of half angles of divergence investigated here do not display a downflow–upflow recirculation loop. It may be conjectured that this deficiency is due to the model employed in ref. [2]. That model did not include the fluid environment in which the flow channel is situated. It is the opinion of the present authors that the inclusion of the environment in the computational model is a necessary step for the attainment of realistic fluid flow patterns.

It was noted earlier that Fig. 2 depicts a quasi-steady picture of the flow field configuration. The actual configuration evolved with time in that the degree of penetration of the recirculation loop into the flow channel became greater as time passed. To illustrate this movement, the timewise variation of the position of point A (the point of deepest penetration) is plotted in Fig. 3. The ordinate is Z_A, the vertical

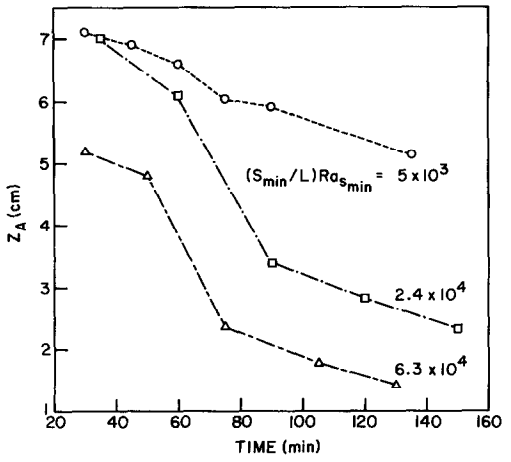

FIG. 3. Timewise penetration of the recirculation zone into the flow channel.

distance between point A and the lower opening of the channel, and the abscissa is the elapsed time in minutes from the beginning of the data run. Note that the times plotted in Fig. 3 all exceed the 15 min period during which data were collected for the evaluation of the reported heat transfer coefficients and Nusselt numbers.

The results in Fig. 3 are specific to $\theta = 15°$ and $L/S_{min} = 11.4$, but they are representative of all the other operating conditions of the experiments. The three sets of data shown in the figure correspond to three different values of the wall-to-ambient temperature difference $(T_w - T_\infty)$, which are reflected in the values of the dimensionless parameter $(S_{min}/L)Ra_{S_{min}}$.

The figure confirms the timewise deeper penetration of the recirculation zone. The extent of the penetration is heightened as the temperature difference $(T_w - T_\infty)$ increases. In particular, for the largest temperature difference (largest value of the curve parameter), the recirculation zone had penetrated quite near to the bottom of the channel at the end of the visualization run (time = 130 min).

Despite the aforementioned timewise change in the flow field configuration, the heat transfer coefficients were constant with time. This is reflected in Fig. 4, where $(T_w - T_\infty)$ is plotted as a function of time for the same cases as were depicted in Fig. 3. It is seen from the figure that $(T_w - T_\infty)$ is independent of time. Since the rate of heat transfer was also time invariant (constant input of electric power), the constancy of the heat transfer coefficient follows directly.

The fact that the heat transfer coefficients were constant despite the progressive intrusion of the recirculation zone into the channel is worthy of note. From this finding, it can be concluded that the heat transfer coefficients are insensitive to happenings which occur outside of the boundary layers. This conclusion will be revisited when the heat transfer coefficients for divergent and convergent channels are compared.

HEAT TRANSFER RESULTS

The average heat transfer coefficient for the flow channel was evaluated from

$$h = Q/A(T_w - T_\infty). \quad (1)$$

Here, Q is the power input to the two heated walls of the channel, and A is the corresponding heat transfer surface area. The wall temperature T_w is the average of the outputs of the thermocouples in the two plates (eight thermocouples in each plate), and T_∞ the average of the three thermocouples in the fluid environment. As already noted, near uniformity of the respective temperatures prevailed during the period of data collection. Heat losses from the rear faces of the plates were estimated to be negligible, so that no corrections were made in evaluating Q.

The Nusselt and Rayleigh numbers are to be used in presenting the heat transfer data. In the search for the most encompassing correlation, the role of various characteristic dimensions will be examined. Therefore, for now, the dimensionless groups will be defined using an arbitrary dimension ξ, that is

$$Nu_\xi = h\xi/k, \quad Ra_\xi = [g\beta(T_w - T_\infty)\xi^3/\nu^2]Pr. \quad (2)$$

In the subsequent presentation of results, ξ will be successively associated with S_{min}, S_{av}, and S_{max}. The thermophysical properties were evaluated at a reference temperature $(T_w + T_\infty)/2$ using algebraic representations given in ref. [3]. The Prandtl number was also evaluated in this way. For all cases, the value of the Prandtl number was close to 5.

Before beginning the presentation of the divergent-channel results, brief consideration will be given to the case of the parallel-walled channel. In the first phase of this research project [1], experimentally determined Nusselt numbers for the parallel-walled case were presented and compared both with prior experimental results and with numerical solutions. These comparisons yielded excellent agreement. In light of the foregoing, there is no need for further discussion of the parallel-walled channel. The Nusselt number results for that case were very well correlated by

$$Nu_S = 0.740[(S/L)Ra_S]^{0.240} \quad (3)$$

where S is the interwall spacing.

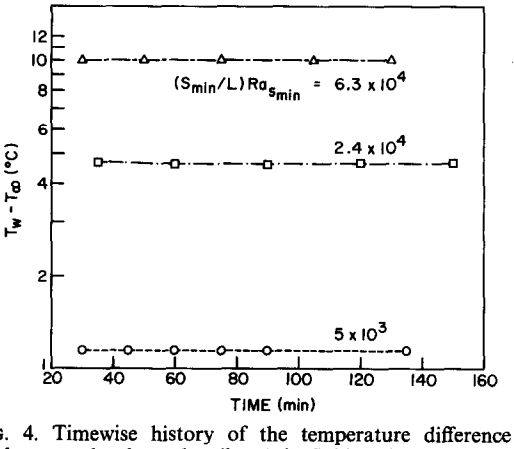

FIG. 4. Timewise history of the temperature difference between the channel wall and the fluid environment.

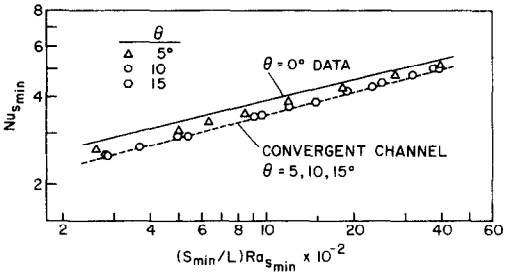

FIG. 5. S_{min}-Based Nusselt number presentation for divergent, convergent, and parallel-walled channels; $L/S_{min} = 22.9$.

The first presentation of the divergent-channel results is made using S_{min} as the characteristic dimension in the participating dimensionless groups. In terms of $(S_{min}/L)Ra_{S_{min}}$ as the abscissa variable, the data for the $L/S_{min} = 11.4$ and 22.9 channels do not overlap and are, therefore, plotted in separate figures.

Figure 5 is for the $L/S_{min} = 22.9$ channel. The divergent-channel results are shown as discrete data points, respectively for half angles of divergence of 5, 10, and 15°. Also appearing in the figure is a solid line which represents the parallel-walled channel correlation of equation (3). In addition, there is a dashed line representing the convergent-channel results of ref. [1]. The convergent-channel Nusselt numbers for half angles of convergence of 5, 10, and 15° were found to be virtually coincident, so that a single line serves for their representation.

From the figure, it is seen that the 10 and 15° divergent-channel data are not only in close agreement with each other but are also in excellent agreement with the 10 and 15° convergent-channel data. This agreement of the divergent- and convergent-channel results is a major finding, but elaboration will be reserved until the presentation of the results has been completed.

The 5° half angle Nu data for the divergent channel do not fall together with the 10 and 15° data, in contrast with the convergent channel. For the 5° case, the divergent-channel Nu exceed those for the convergent channel by 5–8% in the investigated range, with decreasing deviations as $(S_{min}/L)Ra_{S_{min}}$ increases.

The Nusselt numbers for both the divergent and convergent channels fall below those for the parallel-walled channel, with deviations which decrease with increasing values of $(S_{min}/L)Ra_{S_{min}}$. For instance, for $\theta = 10$ and 15°, the deviations range from 13 to 8%.

An overview of Fig. 5 suggests that, at least in the range of the figure, the use of S_{min} as the characteristic dimension does not yield a universal representation of the results for divergent, convergent, and parallel-walled channels. There is, however, a clear trend toward a tighter correlation as $(S_{min}/L)Ra_{S_{min}}$ increases.

Larger values of $(S_{min}/L)Ra_{S_{min}}$ are provided by Fig. 6, which corresponds to $L/S_{min} = 11.4$. The figure is similar in form to Fig. 5, with the divergent-channel results shown as discrete points, while those for the convergent and parallel-walled channels are represented by lines. Note that there is a very slight separation (~2%) between the 5° and 10, 15° representations for the convergent channel.

Figure 6 displays excellent agreement between the divergent- and convergent-channel results. Indeed, the two types of channels appear to be indistinguishable in this figure. Furthermore, the 5, 10, and 15° results fall so closely together that they may be regarded as comprising a single data set. However, the results for the divergent and convergent channels continue to fall below those for the parallel-walled channel, but, clearly, the deviations are diminishing with increasing abscissa values. Over the abscissa range of Fig. 6, the deviations vary from about 8 to 5%.

An overall appraisal of Figs. 5 and 6 indicates that for a sloping-walled channel with a minimum inter-wall spacing S_{min}, the heat transfer coefficient will be moderately lower than that for a parallel-walled channel the (uniform) spacing of which is equal to S_{min}. The dimensionless groupings used in these figures (i.e. based on S_{min}) have been moderately successful in bringing together the results for the three types of channels, but the fact that the parallel-walled Nusselt number results are always above, rather than intermediate to, the others is somewhat troublesome. This provides the impetus to examine the outcome of using either S_{av} or S_{max} as the characteristic dimension.

In particular, the focus of the next two figures is to discern whether the use of either S_{av} or S_{max} can shift the data so that the parallel-walled results fall intermediate to those for the sloping-walled channels. This appraisal will first be performed for the divergent-walled channel, which is, after all, the new case that is reported in the paper. Once it is established which characteristic dimension gives the tightest correlation of the divergent-channel and parallel-channel results, then the convergent-channel results will be reconsidered in order to achieve the most encompassing correlation for all three types of channels.

Figure 7 conveys a presentation of the divergent-channel Nusselt number results in terms of S_{av} as the characteristic dimension in both the ordinate and abscissa variables. In particular, in terms of the $(S_{av}/L)Ra_{S_{av}}$ abscissa variable, the data for the

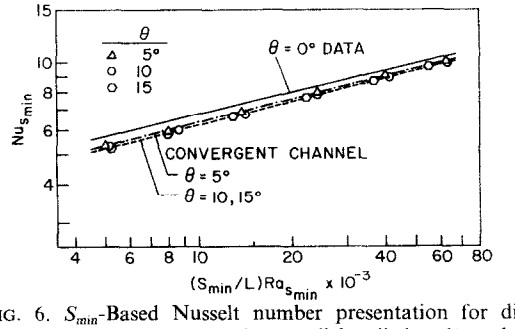

FIG. 6. S_{min}-Based Nusselt number presentation for divergent, convergent, and parallel-walled channels; $L/S_{min} = 11.4$.

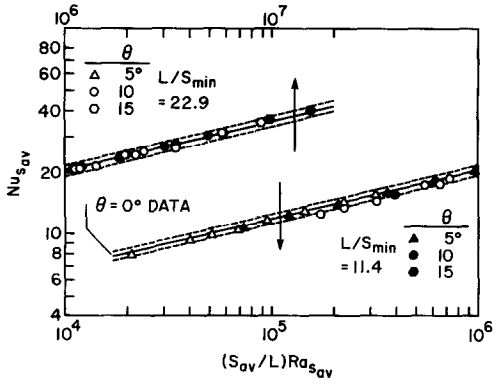

FIG. 7. S_{av}-Based Nusselt number presentation for divergent and parallel-walled channels.

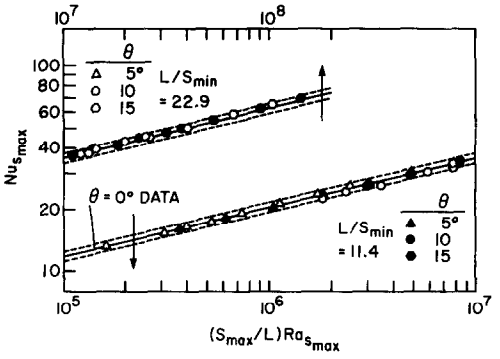

FIG. 8. S_{max}-Based Nusselt number presentation for divergent and parallel-walled channels.

$L/S_{min} = 11.4$ and 22.9 channels overlap, so that it is appropriate to plot them in a single figure. Indeed, the data for the two channel aspect ratios are so intermingled that they appear to constitute a single set. Therefore, in terms of the presentation parameters of the figure, L/S_{min} no longer is an independent parameter.

In addition to the divergent-channel data, Fig. 7 includes a solid line which represents the parallel-walled-channel Nusselt number results of equation (3). The solid line is flanked above and below by dashed lines which are respectively displaced by $\pm 5\%$ from it.

Inspection of the figure indicates that considerable progress has been made in achieving a correlation that is universal for the divergent and parallel-walled channels. In particular, some of the divergent-channel *Nu* data fall above the parallel-channel line, and most of the data lie within 5% of the line. There is, however, room for improvement in that the majority of the data are below the line (albeit not far below) and that there are a few points with greater than 5% deviations from it.

The search for a still tighter correlation is continued in Fig. 8, where S_{max} is used as the characteristic dimension. Otherwise, the format of Fig. 8 is identical to that of Fig. 7. Examination of Fig. 8 and comparison with Fig. 7 indicates that the desired improvements in the correlation have been achieved by the use of S_{max} as the characteristic dimension. In Fig. 8, approximately as many divergent-channel *Nu* data points fall above the parallel-channel line as fall below it. Furthermore, all the divergent-channel data lie within 5% of the line. Also, as was true in Fig. 7, data do not display a separate dependence on the aspect ratio L/S_{min}.

In ref. [1], it was also found that the use of S_{max} as the characteristic dimension gave the tightest correlation of the convergent and parallel-channel Nusselt numbers, relative to that obtainable with the use of S_{min} and S_{av}. It is, therefore, appropriate to use the S_{max}-based variables in the final correlation of the divergent, convergent, and parallel-channel Nusselt number results. This is accomplished in Fig. 9. This figure is similar in format to Fig. 8. The divergent-channel data for all θ and L/S_{min} are represented by circle symbols, while all the convergent-channel data are represented by square symbols.

An overview of Fig. 9 reveals that the goal of unifying the divergent, convergent, and parallel-channel Nusselt number results has been accomplished. The data for the divergent and convergent channels are well intermingled, and the line representing the parallel-channel results passes intermediate to the data. Aside from a few isolated convergent-channel data points, all of the data fall within 5% of the parallel-channel line. This suggests that the parallel-channel correlation of equation (3), when rephrased in terms of the variables of Fig. 9, can serve as a universal representation of the results for sloping-walled (i.e. either divergent or convergent) and parallel-walled channels. After the rephrasing, the universal correlation emerges as

$$Nu_{S_{max}} = 0.740[(S_{max}/L)Ra_{S_{max}}]^{0.240}. \quad (4)$$

Strictly speaking, the correlation conveyed by equation (4) is limited to the ranges of θ, L/S_{min}, and $(S_{max}/L)Ra_{S_{max}}$ encompassed by the present experiments and those of ref. [1]. However, the virtual coincidence of the data for $\theta = 10$ and 15° suggests that extrapolation to larger angles, say 20 or 25°, is permissible. Similarly, the insensitivity of the results to L/S_{min} suggests that

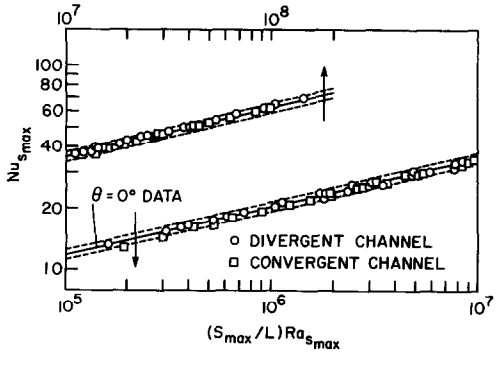

FIG. 9. S_{max}-Based Nusselt number presentation for divergent, convergent, and parallel-walled channels.

substantial extrapolation is allowable, especially since the parallel-channel results are independent of this parameter. With regard to $(S_{max}/L)Ra_{S_{max}}$, inspection of Fig. 9 indicates a slight rising tendency of the data with respect to the correlating line at the high end of the investigated range. At the low end of the range, the convergent-channel data tend to drift below the correlating line. From these observations, it may be conjectured that the correlation could be extended by a factor of 5 with respect to the smallest and largest values of $(S_{max}/L)Ra_{S_{max}}$.

CONCLUDING REMARKS

The dual objectives of collecting definitive divergent-channel heat transfer data and developing a universal correlation for divergent, convergent, and parallel-channel Nusselt numbers have been fulfilled. The universal correlation is conveyed by equation (4), and its range of applicability is discussed in the paragraph which follows the equation.

It remains to discuss the close agreement of the divergent- and convergent-channel Nusselt numbers which prevails despite the significant difference in the patterns of fluid flow in the respective channels. For the divergent channel, the flow visualization performed here indicated the presence of boundary layers adjacent to the channel walls, with a recirculation loop occupying the remainder of the cross section. The boundary layer flow is an upflow. However, in the recirculation loop, the central portion is a downflow and the outer portion is an upflow. Thus, at various cross sections in the divergent channel, there is both upflow and downflow. On the other hand, at all cross sections in the convergent channel, the flow is exclusively an upflow.

The key to rationalizing the close agreement of the Nusselt numbers for the two types of channels is the fact that the divergent-channel Nusselt numbers are insensitive to the flow pattern which prevails outside the boundary layers. It was found here that for a given operating condition (given temperatures and channel geometry), the Nusselt number was independent of the size of the recirculation loop (i.e. the depth of penetration of the recirculation loop into the channel). From this it follows that the presence of the downflow does not affect the divergent-channel Nusselt numbers. Having thus established that the main feature of the divergent-channel flow pattern which differs from the convergent-channel flow pattern is a non-issue, the agreement of the Nusselt numbers for the two channels is more readily accepted.

REFERENCES

1. E. M. Sparrow, R. Ruiz and L. F. A. Azevedo, Experimental and numerical investigation of natural convection in convergent vertical channels, *Int. J. Heat Mass Transfer* **31**, 907–915 (1988).
2. D. Agonafer and C. B. Watkins, Numerical solution of natural convection between diverging plates, ASME Paper 84-WA/HT-32 (1985).
3. R. Ruiz, Natural convection heat transfer in partially enclosed configurations, Ph.D. thesis, Department of Mechanical Engineering, University of Minnesota, Minneapolis, Minnesota (1986).

EXPERIENCES SUR LA CONVECTION NATURELLE DANS DES CANAUX VERTICAUX DIVERGENTS ET FORMULES DES NOMBRES DE NUSSELT POUR DES CANAUX PARALLELES, CONVERGENTS ET DIVERGENTS

Résumé—Cette étude souhaite apporter des données définitives sur le transfert thermique de la convection naturelle dans les canaux verticaux divergents et sur la visualisation de l'écoulement et fournir des formules universelles de nombre de Nusselt pour les canaux à parois parallèles, convergentes et divergentes. Les expériences sont faites avec de l'eau ($Pr \simeq 5$) et elles sont paramétrées avec l'angle de divergence du canal, le rapport de la longueur du canal à la distance minimale et le produit du nombre de Rayleigh par le rapport section droite/longueur. L'uniformité de température est maintenue sur les parois à un niveau supérieur à celui de l'environnement. La visualisation d'écoulement montre la présence d'une zone de recirculation qui s'étend en aval de la sortie dans le canal, mais le nombre de Nusselt est indépendant de l'étendue de la pénétration de la zone de recirculation. Les nombres de Nusselt mesurés pour le canal divergent sont en corrélation étroite avec ceux pour les canaux parallèles et convergents en utilisant des paramètres basés sur l'espacement maximal pris comme dimension caractéristique. La formule est donnée par l'equation (4)

$$(Nu_{S_{max}} = 0{,}740[(S_{max}/L)Ra_{S_{max}}]^{0.240}).$$

EXPERIMENTE ÜBER DIE NATÜRLICHE KONVEKTION IN SICH ÖFFNENDEN SENKRECHTEN KANÄLEN UND KORRELATION DER NUSSELT-ZAHLEN FÜR KANÄLE MIT STEIGENDER, SINKENDER UND GLEICHBLEIBENDER KANALBREITE

Zusammenfassung—Zielsetzung dieser Untersuchung ist die Ermittlung verläßlicher Ergebnisse für den Wärmeübergang bei natürlicher Konvektion in senkrechten Kanälen mit steigender Kanalbreite, außerdem die Sichtbarmachung der Strömungsvorgänge und die Herleitung einer allgemeingültigen Beziehung für die Nusselt-Zahl von Kanälen mit steigender, sinkender und gleichbleibender Kanalbreite. Die Versuche wurden mit Wasser als Arbeitsmedium ($Pr \approx 5$) durchgeführt. Als Parameter wurden der Öffnungswinkel des Kanals, das Verhältnis von Kanallänge zum kleinsten Strömungsquerschnitt und das Produkt aus Rayleigh-Zahl und Querschnittsflächen/Längenverhältnis verwendet. Die Wand des Kanals wurde auf konstanter Temperatur gehalten, die beständig über der Temperatur des strömenden Fluids lag. Die visuelle Beobachtung der Strömung zeigte, daß eine Zone mit Rezirkulation vorhanden ist, welche sich vom Austritt abwärts in den Kanal ausdehnt. Es ergab sich jedoch, daß die Nusselt-Zahl unabhängig von der Ausdehnung dieser Rezirkulationszone ist. Die gemessenen Nusselt-Zahlen für den sich öffnenden Kanal wurden mit denen des sich verengenden und des Kanals mit gleichbleibendem Wandabstand in Beziehung gesetzt, wobei als Parameter der maximale Wandabstand (S_{max}) als charakteristische Dimension verwendet wurde. Die Korrelation ergab die Gleichung:

$$Nu_{S_{max}} = 0{,}740[(S_{max}/L)Ra_{S_{max}}]^{0{,}240}.$$

ЭКСПЕРИМЕНТЫ ПО ЕСТЕСТВЕННОЙ КОНВЕКЦИИ В РАСХОДЯЩИХСЯ ВЕРТИКАЛЬНЫХ КАНАЛАХ И ЧИСЛА НУССЕЛЬТА ДЛЯ РАСХОДЯЩИХСЯ, СХОДЯЩИХСЯ И ПАРАЛЛЕЛЬНЫХ КАНАЛОВ

Аннотация—Данное исследование направлено на получение точных данных по теплопереносу при естественной конвекции в расходящихся вертикальных каналах, визуализацию течения в каналах и вывод универсальной корреляции для чисел Нуссельта для каналов с расходящимися, сходящимися и параллельными стенками. В качестве рабочей жидкости в экспериментах используется вода ($Pr \sim 5$). В качестве характерных параметров экспериментов выбраны величина угла расхождения канала, отношение длины канала к минимальному поперечному сечению, а тежке произведение числа Рэлея на отношение поперечного сечения канала к его длине. На стенках канала поддерживается постоянная температура, причем температура стенок превышает температуру жидкости. При визуализации течения обнаружена рециркуляционная зона, расположенная на входном участке канала. Найдено, что числа Нуссельта не зависят от глубины проникновения рециркуляционной зоны. С помощью комплексов, в которых характерной длиной служит максимальное расстояние между стенками, экспериментальные данные по числам Нуссельта для расходящегося канала удалось описать одним соотношением с числами Нуссельта для каналов со сохдящимися и параллельными стенкацми. Это соотношение имеет вид

$$Nu_{S_{max}} = 0{,}740[(S_{max}/L)Ra_{S_{max}}]^{0{,}240}.$$